Coherent Raman scattering from magnetic excitations in diluted magnetic semiconductors: Bulk crystals of $Cd_{1-x}Mn_xTe$

R. Rupprecht, B. Müller, and H. Pascher
Experimentalphysik I, Universität Bayreuth, D-95440 Bayreuth, Germany

I. Miotkowski and A. K. Ramdas
Department of Physics, Purdue University, West Lafayette, Indiana 47907

(Received 17 November 1997)

Coherent Raman scattering is applied in the investigation of electronic transitions in diluted magnetic semiconductor $Cd_{1-x}Mn_xTe$ bulk crystals ($0.05 \leqslant x \leqslant 0.70$) in the temperature range between 1.7 and 100 K and in magnetic fields B up to 7 T. Free carriers, photoexcited by the high power radiation used, have enabled the observation of the conduction-band free-electron spin flip in alloys nominally free from donors. Apart from the absence of the bound magnetic polaron feature, this free-electron spin-flip transition shows characteristics revealed by the spontaneous Raman scattering from donor bound electrons. Besides the free-electron spin flip, in the regime of large manganese contents ($x \geqslant 0.2$) and low temperatures we observe the Raman antiferromagnetic resonance showing a finite Raman shift at $B=0$, a dependence of the Raman shift linear with magnetic field, corresponding to an effective g factor larger than 2, and a large linewidth up to 3.5 cm^{-1}. For small Mn contents ($x \leqslant 0.2$) and high temperatures, the paramagnetic resonance of electrons within the Zeeman multiplet of the $S=\frac{5}{2}$ ground state of Mn^{2+} is observed. The effective g factor is equal to 2 in this case and the linewidth markedly narrow, e.g., 0.2 cm^{-1} for $x=0.10$. The temperature dependence of the observed Raman shifts connected with magnetic ordering points to a paramagnetic to spin glass phase-transition temperature somewhat below 20 K for $x=0.40$ ($B=6$ T). In contrast, the corresponding linewidths decrease continuously with increasing temperature but remain larger than for $x=0.10$ even at $T=80$ K; the latter sample is paramagnetic in the whole temperature range. [S0163-1829(98)06248-1]

I. INTRODUCTION

A random substitution of the group-IIA element in the tetrahedrally coordinated II-VI semiconductors by a member of the $3d$ transition metals results in a class of ternaries known as diluted magnetic semiconductors (DMS's).[1] The unique coexistence of tunable semiconducting and magnetic properties they possess has provided the motivation for comprehensive optical, transport, and calorimetric studies on these ternaries.[2] Thanks to the large composition range over which it occurs and the simplicity of its structure, the zinc-blende ternary $Cd_{1-x}Mn_xTe$ has served as a prototype of a DMS in numerous investigations for close to two decades. In common with all the II-VI DMS's, there are two types of exchange interactions in $Cd_{1-x}Mn_xTe$. (i) Spin-spin exchange interaction between the d electrons of Mn^{2+} ions on the one hand and those of the s-like (p-like) conduction-(valence-) band states on the other—the so-called *sp-d exchange interaction*. (ii) *Antiferromagnetic d-d coupling* between the magnetic moments of the Mn^{2+} ions.[1] For dilute concentrations ($x \leqslant 0.2$), the Mn^{2+} ions are essentially independent, whereas for larger x and sufficiently low temperatures T, the d-d coupling induces a magnetic order and the system experiences a paramagnetic to spin glass (or antiferromagnetic) phase transition, the transition temperature being concentration dependent.[3]

A huge excitonic Zeeman effect,[4] a giant Faraday effect,[4,5] and a pronounced Voigt effect[6] are the magneto-optic phenomena displayed in a particularly spectacular manner by the II-VI DMS; they can be traced to the strong sp-d interaction mentioned above. Electronic transitions within the Zeeman multiplet of the ground state of magnetic ions such as Mn^{2+} and Co^{2+}, i.e., electron paramagnetic resonance, manifest themselves as Raman shifts (Raman-EPR).[7–9] At sufficiently high concentration of the magnetic ions and low enough temperature, one can observe the collective precession of the magnetic moments of the magnetic ions as an antiferromagnetic Raman line, which is indeed the Raman-antiferromagnetic resonance (Raman-AFMR).[8,10] The spin flip of electrons bound to donors (SF) in large, effective-mass orbits is yet another excitation observed in the Raman spectroscopy of DMS's (Refs. 11–14) in a striking manner.

Coherent second Stokes Raman spectroscopy (CSRS) and coherent anti-Stokes Raman spectroscopy (CARS) are two spectroscopic techniques[15–17] based on high-power lasers which can be applied to the investigation of Raman active excitations. The following special experimental advantages for such coherent Raman spectroscopy (CRS) can be identified in comparing it with spontaneous Raman spectroscopy: (i) The high power of the lasers used in the CRS experiments generates photoexcited free carriers which can be captured by the ionized donors (acceptors). Spin flip of donor-bound electrons (acceptor-bound holes) even in compensated DMS's can thus be studied with a steady-state population of neutral donors (acceptors) using CRS. CRS from free carriers thus generated in the DMS's is equally of interest. (ii) The CRS technique allows the detection of even small shifts. (iii) The spectral resolution accessible with CRS

depends only on the linewidth of the exciting laser light; in our experiments it is as low as 0.05 cm^{-1}. As we shall see, besides the Raman shift, the linewidth of the Raman line provides an important clue in distinguishing Raman-EPR from Raman-AFMR. We note that the detailed knowledge of the physical properties of bulk $Cd_{1-x}Mn_xTe$, in particular those of CRS spectra, is of extreme importance for the interpretation of CRS experiments in II-VI superlattices, e.g., CdTe/MnTe; the magnetic ordering in such systems is of considerable current interest.[18]

In the present paper we report and discuss the CSRS spectra in bulk $Cd_{1-x}Mn_xTe$ associated with (i) the spin flip of the $3d$ electrons of Mn^{2+} in its ground state, (ii) the conduction-band free-electron spin resonance, (iii) the Raman antiferromagnetic resonance, and their behavior as a function of Mn^{2+} concentration (x), temperature (T), and magnetic field (B).

II. COHERENT RAMAN SCATTERING

The coherent Raman scattering techniques CARS and CSRS are types of optical four-wave mixing spectroscopy, where two laser beams with frequencies ω_L and ω_S are superimposed in a sample. Two photons of one laser beam and one of the other interact and generate radiation with new frequencies: $\omega_{\mathrm{CARS}}=2\omega_L-\omega_S$ or $\omega_{\mathrm{CSRS}}=2\omega_S-\omega_L$ ($\omega_L>\omega_S$).[17]

If one identifies ω_L with the pump laser frequency of a conventional Raman experiment and ω_S with the scattered Stokes radiation frequency, corresponding to a Raman shift $\Delta\omega=\omega_L-\omega_S$, then the frequency ω_{CARS} is just the anti-Stokes frequency $\omega_L+\Delta\omega$ and $\omega_{\mathrm{CSRS}}=\omega_S-\Delta\omega=\omega_L-2\Delta\omega$ is the second Stokes frequency.

The output intensity of the CRS radiation[17] is proportional to the square of the length of the sample, to a phase factor resulting from the **k**- conservation rule ($\mathbf{k}_{\mathrm{AS}}=2\mathbf{k}_L-\mathbf{k}_S$), and to the square of the third-order nonlinear susceptibility $\chi^{(3)}$, which contains all the specific properties of the semiconductor material under consideration. Usually in four-wave mixing experiments the **k** conservation is satisfied by noncollinear phase matching. Since in most of our cases the sample length is smaller than the coherence length for collinear beams, we used a collinear geometry which is easier to align, particularly when the laser frequencies are tuned.

The tensor elements $\chi^{(3)}_{ijkl}$ can be calculated by time-dependent perturbation theory describing the interaction between the radiation field and matter.[17] The result is a sum, running over all states $|b\rangle$, $|c\rangle$, and $|d\rangle$ of the system under consideration as intermediate states; in the sum, 24 terms like the one given in Eq. (1) have to be added:

$$\chi^{(3)}_{ijkl}(-\omega_{\mathrm{CARS}},\omega_L,-\omega_S,\omega_L)\propto N_a\times\sum_{|b\rangle,|c\rangle,|d\rangle}\left[\frac{\mu^i_{ab}\mu^j_{bc}\mu^k_{cd}\mu^l_{da}}{[\omega_{ba}-\omega_L-i\Gamma_{ba}][\omega_{ca}-(\omega_L-\omega_S)-i\Gamma_{ca}][\omega_{da}-\omega_{\mathrm{CARS}}-i\Gamma_{da}]}+\cdots\right], \quad (1)$$

where N_a denotes number of quasiparticles (e.g., carriers) occupying the ground state $|a\rangle$. In the numerator, there is a product of four dipole matrix elements $\mu^{\xi}_{\alpha\beta}$, the square of each describing the transition probability between an initial state $|\alpha\rangle$ and a final state $|\beta\rangle$ for a photon with polarization in the ξ direction. In the denominator, $\hbar\omega_{\alpha\beta}$ are energy differences of system states and the phenomenological parameters $\Gamma_{\alpha\beta}$ describe a homogeneous line broadening of the respective resonances. Note, the formulas for CARS and CSRS are symmetric in ω_L and ω_S.[15] $\chi^{(3)}$ has resonances when at least one factor in the denominator gets a small real part and therefore a non-negligible imaginary part.

As discussed in the literature (e.g., Ref. 17), $\chi^{(3)}$ can be split into a resonant part χ_r, which is obtained by separating and summing up all the resonant terms, the remaining terms yielding an additive nonresonant part, χ_{nr}, which approximately can be considered to be a real quantity. χ_r exhibits Raman-like resonances whenever $\hbar(\omega_L-\omega_S)$ is equal to the excitation energy of a Raman allowed transition [see the second factor in the denominator of Eq. (1)]. Furthermore, one-photon resonances may occur, if the laser frequency ω_L corresponds to the energy of a real electronic transition, e.g., an allowed interband transition. If resonances of the first and second term in the denominator of Eq. (1) occur simultaneously, one talks about resonance CARS.

The polarization selection rules for all four one-photon transitions which are involved in the four-photon process have to be fulfilled in order to obtain a nonzero product of four dipole matrix elements, therefore making it possible to observe, e.g., Raman resonances in a CARS experiment. Considering the above-mentioned correspondence of ω_L and ω_S to pump and Stokes radiation of spontaneous Raman scattering, the selection rules can easily be obtained from the ones applying for that. For electronic Raman processes in DMS's, these are discussed in detail by Ramdas and Rodriguez in Ref. 1. In the case of the conduction-band free-electron spin resonance (CSF), as well as EPR and AFMR, two collinear laser beams ($\mathbf{k}_L/|\mathbf{k}_L|=\mathbf{k}_S/|\mathbf{k}_S|\equiv\mathbf{k}$) may be polarized linearly and perpendicular to each other (ω_L: $\mathbf{E}_L\perp\mathbf{B}$, ω_S: $\mathbf{E}_S\parallel\mathbf{B}$) in Voigt configuration ($\mathbf{B}\perp\mathbf{k}$) to observe in a CRS experiment these resonances. CSF satisfies the condition

$$\hbar(\omega_L-\omega_S)=g^*\mu_B B_{\mathrm{res}}. \quad (2)$$

As a consequence of the proportionality $I_{\mathrm{CRS}}\propto|\chi^{(3)}|^2$, the interference of the nonresonant part of $\chi^{(3)}$ and the real part χ'_r of the resonant contribution causes complicated line shapes,

$$\begin{aligned}|\chi^{(3)}|^2&=|\chi_{\mathrm{nr}}+\chi_r|^2=|\chi_{\mathrm{nr}}+\chi'_r+i\chi''_r|^2\\&=|\chi_{\mathrm{nr}}|^2+|\chi_r|^2+2\chi_{\mathrm{nr}}\chi'_r\end{aligned} \quad (3)$$

and therefore the exact resonance positions of the observed Raman lines have to be found by a line-shape fitting procedure.[19,20]

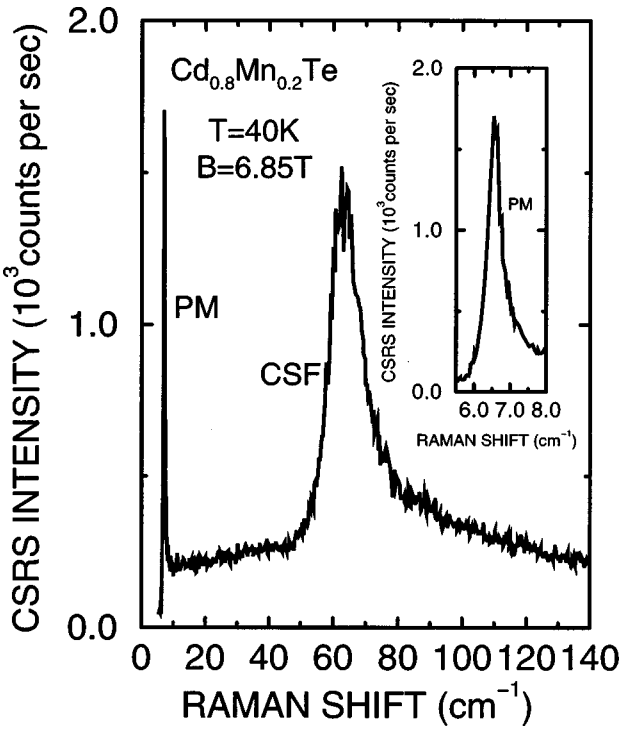

FIG. 1. CSRS spectrum (CSRS intensity vs Raman shift $\Delta\omega$) of $Cd_{0.8}Mn_{0.2}Te$ for $B=6.85$ T and $T=40$ K. PM denotes the paramagnetic resonance of the Mn^{2+} $3d^5$ electrons, CSF denotes the conduction-band free-electron spin resonance. The inset shows the PM region with an extended scale on the x axis.

In order to take advantage of band-gap resonances of the CARS signal, we have done resonance CRS experiments with tunable laser sources, opening the possibility to enhance the output signal intensity by several orders of magnitude.

III. EXPERIMENT

Our samples of $Cd_{1-x}Mn_xTe$ were grown by a modified vertical Bridgman method. Small slabs with a thickness of about 1 mm were cut and the faces polished to optical quality. In the composition range $0 \leqslant x \leqslant 0.7$, the DMS alloy crystal $Cd_{1-x}Mn_xTe$ is known to crystallize in the cubic zinc-blende structure. Samples in the range $x=0.05$ to 0.7 (nominal) were investigated in the present work.

To excite the coherent Raman spectra, we use two dye lasers (CONTINUUM, TDL 60) which are simultaneously pumped by the second harmonic of a 50 Hz Q-switched Nd:YAG laser (CONTINUUM YG 681-50). A special optical layout of the dye laser cavities, the so-called Moya design,[21] ensures a low background fluorescence. Using two gratings under grazing incidence, one obtains a spectral laser linewidth down to 0.05 cm^{-1} without etalons in the cavity. These specifications are of particular interest doing CRS experiments, because in this case the spectral resolution obtainable depends only on the linewidths of the exciting laser light.

In order to fulfill the selection rules for spin-flip Raman resonances, the polarization of the radiation of one of the exciting lasers has to be rotated by 90°, which we achieve using a KD*P pockels cell in dc operation. The dye laser beams are then made collinear to each other by means of a calcite crystal and attenuated by several orders of magnitude down to a few microjoules each, before focusing on the samples. These are inserted in Voigt geometry in a 7 T superconducting split-coil magnet system and either immersed in superfluid helium pumped down to $T=1.7$ K or held in a helium gas flow at a stabilized temperature provided by a temperature controller. Experiments of the present investigations were done in the temperature range up to $T=100$ K.

The radiation generated by four-wave mixing is collected in forward direction and then focused onto the entrance slit of a 0.85-m double spectrometer, used to separate the signal from the laser radiation. Note, when doing CRS experiments the spectral resolution obtainable does not depend primarily on the spectrometer resolving power nor is the spectrometer necessary for a determination of the signal wavelength.

The CRS signal is detected by a liquid nitrogen cooled charge-coupled device (CCD) camera. Besides a very low dark current of only a few electrons per minute and a maximum quantum efficiency of about 50%, this 512×512 pixel detector chip offers a unique property as compared to a photomultiplier system: working without a spectrometer exit slit, a relatively large wave-number range is recorded in one and the same image, e.g., 70 cm^{-1} (at 632 nm) with our apparatus. On this scale a background due to luminescence or remaining stray light is fairly broad in the dispersion direction, whereas the coherent Raman line covers more or less one pixel. Thus even signals having only a small fraction of the mean background intensity can be detected with confidence.

For many subsequent laser frequency differences $\Delta\omega = \omega_L - \omega_s$, such an image is taken and thus the signal intensity at the frequencies ω_{CARS} or ω_{CSRS} as a function of $\Delta\omega$ is recorded. More specifically, the procedure for discovering a CARS (CSRS) resonance consists of recording CCD images in the range of ω_{CARS} (ω_{CSRS}) for successive values of $(\omega_L - \omega_S)$, ω_L being held fixed and ω_S tuned (in steps as small as 0.03 cm^{-1} for the sharp Raman-EPR signal). The absolute intensity of CARS (CSRS) resonances reaches a maximum for $\hbar\omega_L \approx$ energy gap [as can be seen from Eq. (1)]. Thus the choice of ω_L varies with x.

IV. RESULTS AND DISCUSSION

A typical CSRS spectrum of bulk $Cd_{1-x}Mn_xTe$ is shown in Fig. 1 for $x=0.2$, recorded at a magnetic field (B) of 6.85 T and a temperature (T) of 40 K. A very sharp resonance, but with full width at half maximum (FWHM) of 0.4 cm^{-1} in excess of the instrumental width, occurs with a Raman shift of 6.4 cm^{-1}. The linear shift with B yields an effective g factor (g^*_{PM})≈ 2, consistent with the origin of the line being due to the $\Delta m_J = \pm 1$ transitions within the Zeeman multiplet of the $3d^5$ shell of Mn^{2+} ($L=0$, $S=\frac{5}{2}$). We therefore label this Raman-electron paramagnetic transition as ''PM.''

Figure 1 also displays a line $\approx$62.5 cm^{-1} labeled ''CSF,'' drastically different from that of the PM line. This is to be contrasted with the spin-flip Raman shift of $\approx$5 cm^{-1} at $B=6.85$ T expected for conduction-band free electrons of bulk CdTe with their intrinsic g factor (g^*) of -1.6 (Ref. 22). The magnetic-field dependence of the CSF Raman line is shown in Fig. 2(a) for $x=0.10$ and 0.20. Note that for both samples, as shown in Fig. 2(b) on an expanded scale, the Raman shift is zero at zero field (see the discussion below).

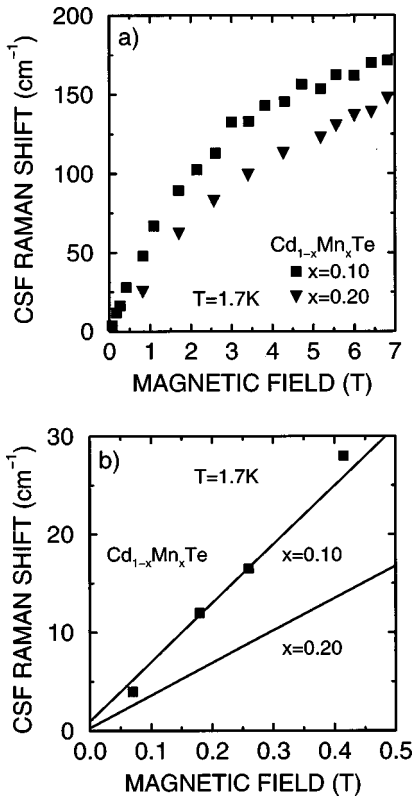

FIG. 2. (a) Raman shift due to the conduction-band free-electron spin resonance at $T=1.7$ K as a function of the magnetic field for $Cd_{1-x}Mn_xTe$, $x=0.10$ (upper trace) and $x=0.20$ (lower trace). (b) The CSF Raman shifts in (a) are shown here on an expanded scale; the figure emphasizes that the Raman shift for $B=0$ is, within experimental errors, zero. The straight lines are least-squares fits to the data up to $B=1$ T for $x=0.1$ and $B=3$ T for $x=0.2$, respectively.

The Raman shift for $x=0.10$ is consistently higher than that for $x=0.20$. A saturation of the Raman shift as a function of magnetic field is observed for both samples. We ascribe this Raman line to the spin flip of the photoexcited free electrons

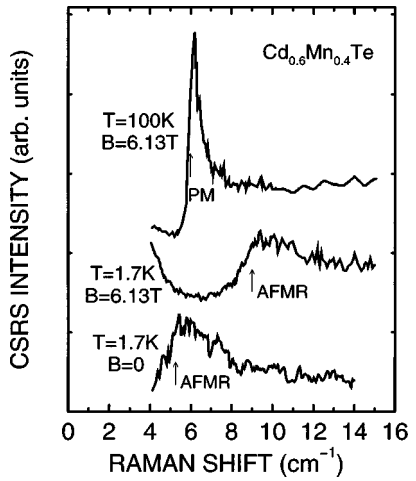

FIG. 3. CSRS spectra of $Cd_{0.6}Mn_{0.4}Te$. Lower trace: Raman antiferromagnetic resonance (AFMR) at $B=0$ and $T=1.7$ K. Second trace: AFMR at $T=1.7$ K and $B=6.13$ T. Upper trace: paramagnetic resonance (PM) at $B=6.13$ T and $T=100$ K. Successive spectra have been shifted upwards for clarity.

in the conduction band in the presence of an external magnetic field, the shift being given[14] by

$$\hbar\omega_0 = x\alpha N_0\langle S_z^{\mathrm{Mn}}\rangle + g^*\mu_B B. \tag{4}$$

Here α = exchange integral of the $3d$ states of Mn^{2+} and conduction electrons; x = fraction of Cd^{2+} ions replaced with Mn^{2+}; $\langle S_z^{\mathrm{Mn}}\rangle$ is the average value of the Mn^{2+} spin along **B** given by $(5/2)B_{5/2}[g\mu_B B/k_B(T+T_{\mathrm{AF}})]$ in the paramagnetic phase; N_0 = density of cations; μ_B = Bohr magneton.

The CRS is attributed to the spin flip of free electrons in the conduction band, photoexcited by the high power of the lasers in adequate density for the Raman signal to be detected; even with photon energies smaller than the band gap, two-photon absorption can generate such carriers in sufficient numbers.[23] In contrast to spontaneous spin-flip Raman scattering from $Cd_{1-x}Mn_xTe$ intentionally doped with donors, e.g., $Cd_{1-x}Mn_xTe$(Ga),[14] where one observed bound magnetic polarons (BMP), we can explore here ''free magnetic polaron'' (FMP) effects. A signature of the BMP effect is the occurrence of a zero-field spin-flip Raman line. According to Dietl and Spalek,[24,25] ''the electron localized on a donor in a DMS polarizes the magnetic ions within its orbit, creating a spin cloud that exhibits a new magnetic moment. An additional effect on the binding energy of the electron bound to the donor originates from thermodynamic fluctuations of the magnetization and the resulting spin alignment of the magnetic ions around the donor.'' In our experiments the spin-flip Raman shift extrapolates to zero for $B=0$. In order to illustrate clearly that the spin-flip Raman shift of photoexcited free electrons, i.e., $\hbar\omega_0$ in Eq. (4), is zero for $B=0$, we display in Fig. 2(b) $\hbar\omega_0$ for $x=0.1$ in the range $0\leqslant B\leqslant 0.5$ T; a linear least-squares fit for the lowest six values of $\hbar\omega_0$ (including the two above $B=0.5$ T) extrapolates to ≈ 1 cm^{-1}. This is to be contrasted with 5 cm^{-1} for $Cd_{1-x}Mn_xTe$(Ga), $x=0.1$, obtained by Peterson *et al.*[14] The results for $x=0.2$ extrapolate to ≈ 0.3 cm^{-1} using $\hbar\omega_0$ values up to $B=3$ T. A separate measurement in the range up to 5 cm^{-1} also did not show a spin-flip Raman line at $B=0$, supporting the inference that the CSF resonances are not associated with magnetic polaron effects. The absence of a BMP feature testifies to the high structural quality and chemical purity of our samples, on the one hand, and the lack of magnetically self-trapped carriers is consistent with the calculations of Benoit à la Guillaume[26] on the other. The smaller Raman shift for $x=0.2$ than for $x=0.1$ noted above arises from the larger number of antiferromagnetically coupled, nearest-neighbor Mn^{2+} ions in the former, thus eliminating their contribution.

As mentioned in the Introduction, II-VI DMS's become magnetically ordered at low temperatures and for sufficiently large concentration of the magnetic ion. For bulk $Cd_{1-x}Mn_xTe$, such a magnetically ordered phase was discovered by Galazka *et al.*[27] for $x>0.17$. The magnetic ordering is a consequence of the d-d interaction which is antiferromagnetic.[3,28]

The coordinates describing the elementary excitations of a system of interacting magnetic dipoles—the magnons—can be regarded as the Fourier components of the magnetization $M(r,t)$, i.e., the coefficients M_q in the expansion

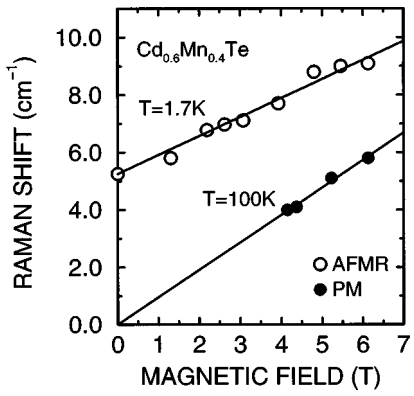

FIG. 4. Raman shift as a function of magnetic field for $Cd_{0.6}Mn_{0.4}Te$. Upper trace at $T=1.7$ K: AFMR. Lower trace at $T=100$ K: PM.

$$M(r,t)=\sum_q M_q \exp(iqr-i\omega_q t). \tag{5}$$

In first-order Raman scattering, only the long-wavelength magnons can be excited. The description of such an excitation as it pertains to $Cd_{1-x}Mn_xTe$ and the selection rules and polarization features to be expected for its appearance in spontaneous Raman scattering (Raman-AFMR) are given by Ramdas and Rodriguez.[29] In the CSRS spectrum of a $Cd_{0.6}Mn_{0.4}Te$ bulk specimen, indeed, the Raman-AFMR feature appears at 1.7 K in the magnetically ordered low-temperature phase, as can be seen in the lowest trace of Fig. 3. Absent in the paramagnetic phase, the AFMR feature makes its appearance at the lower temperature and higher manganese concentration. The Raman shift increases with increasing field. From the $2\chi_{nr}\chi_r'$ term in Eq. (3), the CSRS line shape given by the real part of the susceptibility occurs. As can be seen in the figure, the AFMR signature transforms into that of PM as the temperature increases and the system is driven into the paramagnetic phase. The PM signature is significantly narrower, with a much smaller Raman shift for the same magnetic field; as noted earlier, it is characterized by $g^*_{PM}=2$. The AFMR feature also exhibits a linear dependence of the Raman shift above the $B=0$ value—it extrapolates precisely to it as the magnetic field is reduced, as can be seen in Fig. 4.

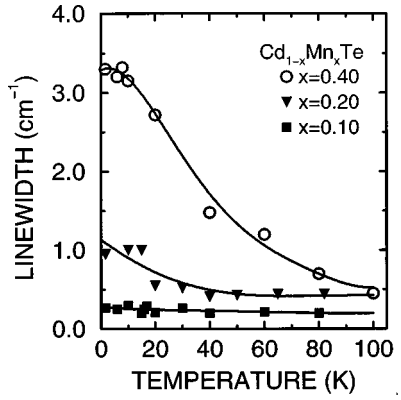

FIG. 5. Temperature dependence of the Raman linewidths for $Cd_{1-x}Mn_xTe$, $x=0.40$, 0.20, and 0.10, respectively (from top to bottom). Solid lines are guides for the eyes.

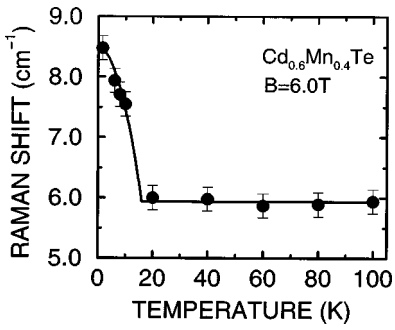

FIG. 6. Resonance frequency of the AFMR and PM features as a function of temperature for $Cd_{0.6}Mn_{0.4}Te$ at $B=6.0$ T. In the range $T\geqslant 17$ K, the solid line corresponds to an effective g factor of 2 (PM). For $T\leqslant 17$ K, the solid line is a guide for the eyes and does not correspond to a theoretical model.

The CSRS linewidths as a function of temperature are quantitatively compared in Fig. 5 for $x=0.1$, 0.2, and 0.4. The decrease in linewidth at the higher temperature is pronounced for $x=0.2$ and 0.4, whereas it is the smallest for $x=0.1$ and remains constant throughout the entire temperature range. The increase in linewidth and Raman shift with decreasing temperature, clearly observed here for $x=0.2$, signals the onset of at least a short-range antiferromagnetic ordering, although the g factor does not show a noticeable increase over 2 throughout the temperature range. As discussed in Ref. 2, for low x or below the percolation limit,[30] the ''antiferromagnetic locking'' would occur at considerably lower temperatures, consistent with the lower values of the exchange integrals for neighbors farther removed. For $x=0.1$, such a ''locking'' process occurs, if at all, well below 1.7 K. In this context, it is interesting to compare the Raman shift in the $x=0.4$ sample as a function of temperature (Fig. 6) with the temperature dependence displayed in Fig. 5. The increase in shift below the Neél temperature $T_N=(17\pm3)$ K and its constant value above it with $g^*_{PM}=2.0$ are the striking features. (These are very strongly reminescent of the spontaneous Raman-AFMR displayed in Fig. 11 of Ref. 8 for $x=0.7$.) It is clear that, with decreasing temperature, the linewidth indicates the onset of the d-d interaction effects well ahead of the establishment of the fully ordered phase.

The first term on the right-hand side of Eq. (4) is proportional to the magnetization of the sample. Thus for fixed B

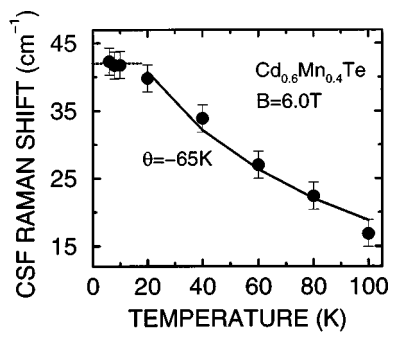

FIG. 7. CSF frequencies at $B=6$ T as a function of temperature for $Cd_{0.6}Mn_{0.4}Te$. Full line: fit to a Curie-Weiss law with $\Theta=-65$ K.

and variable temperature, $\hbar\omega_0 - g^*\mu_B B$ ($\hbar\omega_0$ being the free-electron spin splitting) reflects the temperature dependence of the magnetic susceptibility χ_m. For an antiferromagnet in its paramagnetic phase, the temperature dependence of χ_m is given by the Curie-Weiss law:

$$\chi_m(T) = \frac{C}{T-\Theta} \tag{6}$$

with Curie constant C and paramagnetic Curie temperature Θ. In Fig. 7, the Raman shift due to the free-electron spin resonance is plotted versus temperature for a fixed magnetic field of 6 T. The full line is a fit of Eq. (6) to the experimental data for $T \geqslant 20$ K, resulting in $\Theta = -65$ K. For $T < 20$ K the experimental results are constant, lying below the Curie-Weiss curve. This behavior indicates the onset of an antiferromagnetic coupling between 15 and 20 K, in excellent agreement with the data shown in Fig. 6. In a homogeneous antiferromagnet, from the Neél temperature and Θ, the exchange integrals for nearest- and next-nearest-neighbor interactions can be calculated.[31] However, in the alloy investigated here, the number of nearest- and next-nearest-neighbor magnetic ions differs within antiferromagnetically ordered clusters, making such a calculation challenging.

V. CONCLUDING REMARKS

The high laser powers used in coherent Raman experiments, reported and discussed in the present paper, have enabled the observation of spin resonances of the photoexcited free electrons even in nominally undoped $Cd_{1-x}Mn_xTe$ samples. The dependence of the transition energy on the magnetic field shows at high fields the Brillouin-function-like behavior identical to that of the corresponding spontaneous Raman line in *n*-doped crystals. At low field this dependence extrapolates to zero for vanishing magnetic field. Since our CRS apparatus can detect Raman shifts as small as 2 cm^{-1}, we can state that no finite Raman shift is observed at $B = 0$, i.e., no free magnetic polaron exists, at least not with an energy bigger than 2 cm^{-1}.

The phase transition between paramagnetic and ordered spin glass phase can be deduced from the transition energy of the intra-Mn spin resonance with $g^*_{PM} = 2$ for paramagnetic and $g^*_{AFMR} > 2$ for antiferromagnetic resonance, or from the increased linewidth of the transition in the ordered phase. For the determination of the PM linewidth, the high spectral resolution of the coherent Raman experiment is necessary. While the transition energy as a function of temperature shows a well pronounced transition temperature, the linewidth gradually decreases with increasing temperature. Crystals with $x \geqslant 0.2$ exhibit broader PM lines even at rather high temperatures compared to those with $x \leqslant 0.1$.

ACKNOWLEDGMENTS

R.R., B.M., and H.P. thank the Deutsche Forschungsgemeinschaft (DFG), Bonn, for financial support. I.M. and A.K.R. express their appreciation to the U.S. National Science Foundation (Grant Nos. DMR93-03186 and DMR92-21390) for providing support. A.K.R. and H.P. also acknowledge U.S.–Germany Cooperative Research supported by the U.S. National Science Foundation (9726210-INT) and DAAD (Bonn).

[1] For a general reference, see *Diluted Magnetic Semiconductors*, edited by J. K. Furdyna and J. Kossut, Semiconductors and Semimetals Vol. 25, series editors R. K. Willardson and A. C. Beer (Academic, San Diego, 1988).
[2] J. K. Furdyna, J. Appl. Phys. **64**, R29 (1988).
[3] S. Oseroff and P. H. Keesom, Ref. 1, pp. 73–123.
[4] J. A. Gaj, Ref. 1, pp. 275–309.
[5] E. Oh, A. K. Ramdas, and J. K. Furdyna, J. Lumin. **52**, 183 (1992).
[6] E. Oh, D. U. Bartholomew, A. K. Ramdas, J. K. Furdyna, and U. Debska, Phys. Rev. B **44**, 10 551 (1991).
[7] A. Petrou, D. L. Peterson, S. Venugopalan, R. R. Galazka, A. K. Ramdas, and S. Rodriguez, Phys. Rev. Lett. **48**, 1036 (1982).
[8] A. Petrou, D. L. Peterson, S. Venugopalan, R. R. Galazka, A. K. Ramdas, and S. Rodriguez, Phys. Rev. B **27**, 3471 (1983).
[9] J. Stühler, M. Hirsch, G. Schaak, and A. Waag, Phys. Rev. B **49**, 7345 (1994).
[10] S. Venugopalan, A. Petrou, R. R. Galazka, and A. K. Ramdas, Solid State Commun. **38**, 365 (1981).
[11] F. F. Geyer and H. Y. Fan, IEEE J. Quantum Electron. **QE-16**, 1365 (1980).
[12] M. Nawrocki, R. Planel, G. Fishman, and R. Galazka, Phys. Rev. Lett. **46**, 735 (1981).
[13] D. L. Peterson, A. Petrou, M. Dutta, A. K. Ramdas, and S. Rodriguez, Solid State Commun. **43**, 667 (1982); D. Heiman, P. A. Wolff, and J. Warnock, Phys. Rev. B **27**, 4848 (1983).
[14] D. L. Peterson, D. U. Bartholomew, U. Debska, A. K. Ramdas, and S. Rodriguez, Phys. Rev. B **32**, 323 (1985).
[15] M. D. Levenson and S. S. Kano, *Introduction to Nonlinear Laser Spectroscopy* (Academic, San Diego, 1987). See Fig. 4.1, p. 131, and the associated discussion in the context of the symmetry of CARS and CSRS with respect to ω_L and ω_S.
[16] M. D. Levenson, C. Flytzanis, and N. Bloembergen, Phys. Rev. B **6**, 3962 (1972).
[17] G. L. Eesley, *Coherent Raman Spectroscopy* (Pergamon, Oxford, 1981).
[18] B. Müller, R. Rupprecht, H. Pascher, W. Faschinger, H. Sitter, G. Bauer, and A. K. Ramdas, Mater. Sci. Forum **182–184**, 767 (1995); R. Rupprecht, H. Pascher, W. Faschinger, H. Sitter, and G. Bauer, J. Cryst. Growth **184/185**, 952 (1998).
[19] S. Y. Yuen and P. A. Wolff, Appl. Phys. Lett. **40**, 457 (1982).
[20] H. Pascher, Appl. Phys. B: Photophys. Laser Chem. **34**, 107 (1984).
[21] Continuum, Operation and Maintenance Manual ND60 Dye Laser (1990).
[22] A. Nakamura, D. Paget, C. Hermann, C. Weisbuch, and G. Lampel, Solid State Commun. **30**, 411 (1979); P. E. Simmonds, H. Venghaus, R. Sooryakumar, and P. J. Dean, *ibid.* **43**, 311 (1982).
[23] F. Geist, H. Pascher, N. Frank, and G. Bauer, Phys. Rev. B **53**, 3820 (1996).
[24] T. Dietl and J. Spalek, Phys. Rev. Lett. **48**, 355 (1982).
[25] T. Dietl and J. Spalek, Phys. Rev. B **28**, 1548 (1983).

[26] C. Benoit à la Guillaume, Phys. Status Solidi B **175**, 369 (1993).
[27] R. R. Galazka, S. Nagata, and P. H. Keesom, Phys. Rev. B **22**, 3344 (1980).
[28] T. Giebultowicz and T. M. Holden, Ref. 1, Chap. 4.
[29] A. K. Ramdas and S. Rodriguez, in *Raman Scattering in Diluted Magnetic Semiconductors in Light Scattering in Solids VI*, edited by M. Cardona and G. Güntherodt (Springer-Verlag, Heidelberg, 1991), pp. 137–206.
[30] L. de Seze, J. Phys. C **10**, L353 (1977).
[31] P. Wachter, CRC Crit. Rev. Solid State Sci. **3**, 189 (1972).